Potassium titanyl phosphate Z- and Y-cut surfaces from density-functional theory

S. Neufeld,* A. Bocchini, and W. G. Schmidt
Lehrstuhl für Theoretische Materialphysik, Universität Paderborn, 33095 Paderborn, Germany

(Received 31 March 2021; accepted 3 June 2021; published 14 June 2021)

While potassium titanyl phosphate (KTP) is widely used for various optics applications, essentially nothing is known about its surfaces and electronic properties. Here the ground-state atomic structures of KTP [001] and [010] surfaces, frequently termed Z and Y cuts, respectively, have been determined using ground-state density-functional theory total-energy calculations. The calculated surface phase diagrams in dependence on the chemical potentials of the materials constituents show several stable nonstoichiometric terminations. A tendency to form oxygen-rich surfaces is observed. The Z^+ and Z^- surfaces, discriminated by oppositely orientated internal electric fields, are found to differ with respect to their stoichiometry and structure. Occupied O-derived and in some cases unoccupied Ti-derived surface states appear in the lower and upper part of the bulk band gap, respectively.

DOI: 10.1103/PhysRevMaterials.5.064407

I. INTRODUCTION

Within the last decades the ferroelectric potassium titanyl phosphate ($KTiOPO_4$, KTP) has become a common material for nonlinear optics applications. Its large optical nonlinearity and homogeneity [1] along with its wide transparency range are utilized for, e.g., waveguide structures [2] and frequency conversion devices [3]. KTP crystallizes in the orthorhombic space group $Pna2_1$ [4]. It is characterized by distorted TiO_6 and PO_4 polyhedra linked by a mutual O atom that form a three-dimensional polyhedra network along [100] and [010]. The cavities of this framework are occupied by K^+ ions, which possess a high mobility along the [001] direction [2]. The large nonlinearity of KTP has been attributed to a number of structural features, including a distortion of Ti–O [1], P–O, and K–O bonds [5]. KTP can be grown by hydrothermal growth [6] and flux methods [7]. Crystals obtained by either method are prone to intrinsic defects, in particular H interstitials [8,9] as well as K and O vacancies [10]. Charged defects of the latter kind have been related to the formation of color centers in KTP (gray tracks) via a reduction of the Ti ions from Ti^{4+} to Ti^{3+} [10,11]. These color centers may form during frequency conversion processes under high-intensity laser irradiation, causing photochromatic damage to the crystal. An emission band at 820 nm in as-grown KTP has been shown to originate from Ti^{3+} centers close to the surface [12].

The displacement of Ti atoms within the TiO_6 octahedra gives rise to a spontaneous polarization along the [001] direction amounting to $P_s = 20.1\ \mu C\ cm^{-2}$ [13,14]. Cutting KTP perpendicular to [001] therefore creates two nonequivalent surfaces (in the following referred to as Z^+ and Z^-). A similar nonequivalence between Z-cut surfaces can be observed for several ferroelectric oxides, e.g., lithium niobate [15]. The surface structure of flux-grown KTP has been studied by Bolt *et al.*, using optical microscopy [16]. The presence of a small number of growth hillocks and microsteps on all KTP faces was noted and traced to a spiral growth mechanism. Similar findings were made for hydrothermally grown KTP [6]. In a study by Nikolaev *et al.*, the formation of periodic nanostructures on KTP surfaces upon Ar ion irradiation has been shown for incident angles $\leqslant 30^\circ$ [17]. Atuchin *et al.* used x-ray photoelectron spectroscopy and reflection high-energy electron diffraction (RHEED) to explore the surface stoichiometry of the Z surface [18,19]. The as-grown face was found to be covered by a thick amorphous layer depleted of K and P. Upon mechanical polishing, this layer vanished and exposed a surface with a chemical composition very close to bulk KTP. Furthermore, the formation of nanosized KTP islands dimensioned $(1 \times 4 \times 4)$ was observed for annealing temperatures of 550 °C at the Z-cut face. Upon further increase in annealing temperature, KTP was found to decompose and anatase TiO_2 nanocrystals formed on the surface.

As far as we know, there is no information available on the equilibrium atomic structure of the KTP surfaces. Also, it is not known to what extent the KTP optical properties are affected by surface electronic states. The present paper is an attempt to address these questions on the basis of density-functional theory (DFT) calculations. *Ab initio* thermodynamics is used to determine the thermodynamically stable surface terminations of the technologically most relevant Z^+, Z^-, and Y-cut surfaces. The surfaces that are most prominent in the calculated surface phase diagrams are investigated with respect to their electronic structures.

II. METHODOLOGY

The total-energy calculations are performed using the Vienna *ab initio* simulation package (VASP) [20] DFT implementation. The electron exchange and correlation energy is calculated within the generalized gradient approximation

*sergejn@mail.upb.de

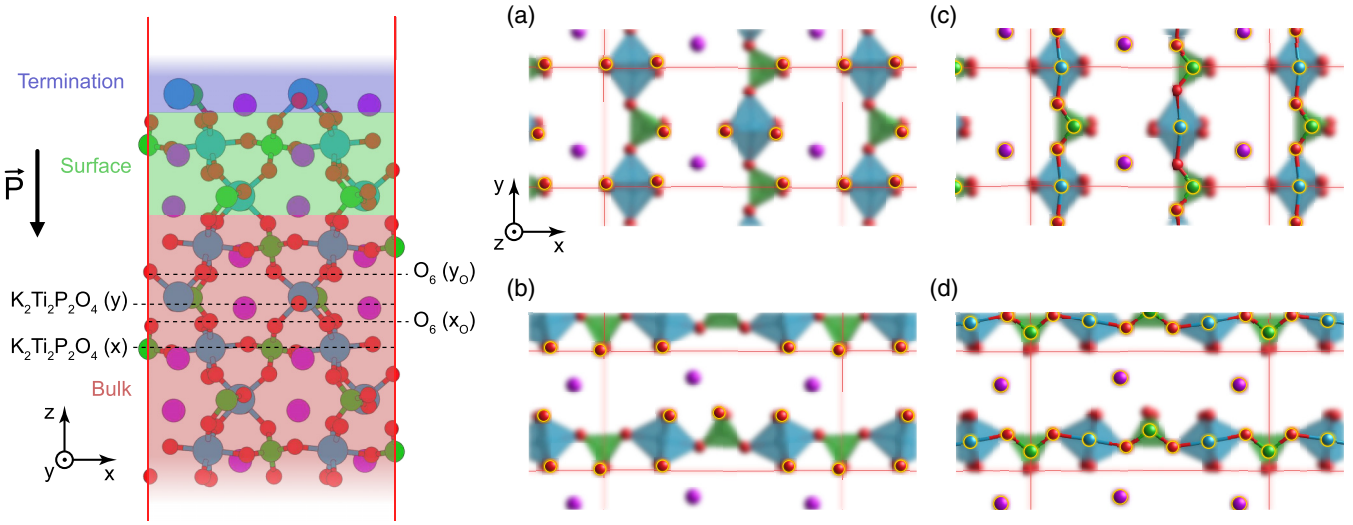

FIG. 1. Left: Stacking sequence of $K_2Ti_2P_2O_4$ and O_6 layers in Z-cut KTP. Bulk layers are kept fixed during relaxation, while all four surface layers as well as the termination atoms are free to relax. K, Ti, P, and O atoms are depicted in purple, blue, green, and red, respectively. The direction of the internal polarization $\vec{P}$ is indicated. Right: Atomic arrangement of bulk cut (a) $O_6(y_O)$, (b) $O_6(x_O)$, (c) $K_2Ti_2P_2O_4(y)$, and (d) $K_2Ti_2P_2O_4(x)$ terminations. Surface atoms are highlighted in yellow.

(GGA) using projector augmented wave potentials (PAW) [21] and the PBEsol functional [22]. All open shells as well as K_{3p}, Ti_{4s}, Ti_{3p}, P_{3s}, and O_{2s} have been considered valence states. PBEsol has been shown to accurately reproduce the experimental lattice constants of KTP, with deviations smaller than 0.4% [23]. The electron wave functions are expanded into plane waves up to an energy cutoff of 500 eV. The Brillouin zone integration is carried out using Γ centered $2 \times 4 \times 1$ and $2 \times 2 \times 1$ k-point meshes for Z-cut and Y-cut surfaces, respectively. The respective Z- and Y-cut surfaces are modeled using periodic repetitions of the orthorhombic KTP unit cell along the z and y direction. The calculations are restricted to the bulk periodicity, i.e., do not allow for the formation of surface reconstructions. The initial coordinates for the calculations are taken from a previous DFT study [23]. Structural relaxation of each considered surface region was performed until the maximum force acting on all atoms fell below a threshold of 0.01 eV/Å.

Along the z direction, KTP may be thought of as assembled of alternating $K_2Ti_2P_2O_4$ and O_6 layers, see Fig. 1. These layers can be further discriminated by the orientation of the constituent TiO_6 and PO_4 polyhedra. These are connected by a common O atom and form chain structures parallel to either the x direction [Figs. 1(b) and 1(d)] or the y direction [Figs. 1 a and 1(c)]. Accordingly, we discriminate here between $K_2Ti_2P_2O_4$ (x) and (y) layers as well as between O_6 (x_O) and (y_O) layers. The Z-cut surfaces are modeled here by 11...14 layers with atom coordinates frozen to the atomic bulk positions and additional four surface layers and one termination layer. The atoms in the surface and termination layers are allowed to relax freely. The bottom layer is chosen as y_O layer with frozen bulk atom coordinates for all Z^+- and Z^--cut surfaces investigated here. In addition to the predominant P–O bonds, KTP is also characterized by highly ionic Ti–O bonds. Therefore, a hydrogen passivation of the bottom layer is not meaningful. However, all slabs used here to model a specific cut share the same bottom layer in order to allow for calculating meaningful energy differences between different surface terminations.

A vacuum layer of 15 Å is used to separate the material slabs along the direction of the surface normal in order to minimize spurious interactions between the surfaces. Dipole corrections along the [001] direction are applied in order to mitigate spurious electric fields arising from electrostatic interactions between the Z^+ and Z^- surfaces.

Along the y direction, KTP can be considered to be composed of alternating $Ti_2P_2O_{12}$ and $K_4Ti_2P_2O_8$ layers, see Fig. 2. Similar to the Z-cut, these layers will, in the following, be abbreviated as z and x, respectively. The Y-cut is nonpolar.

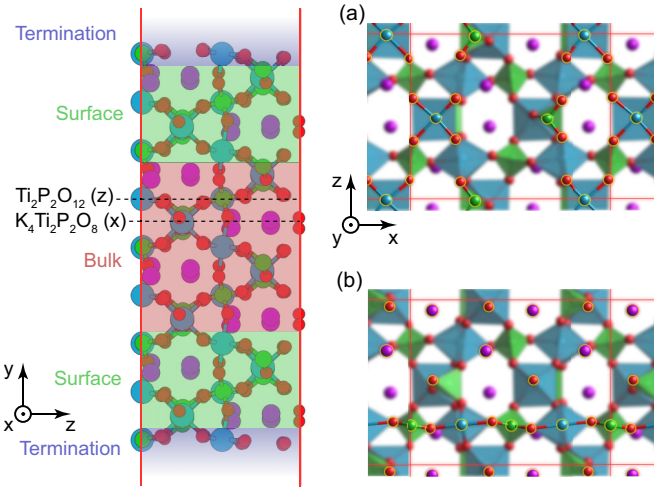

FIG. 2. Left: Stacking sequence of $Ti_2P_2O_{12}$ and $K_4Ti_2P_2O_6$ layers in Y-cut KTP. Bulk layers are kept fixed during relaxation, while all four surface layers as well as the termination atoms are free to relax. The color coding follows Fig. 1. Right: Atomic arrangement of bulk cut (a) $Ti_2P_2O_{12}(z)$ and (b) $K_4Ti_2P_2O_8(x)$ terminations. Surface atoms are highlighted in yellow.

TABLE I. Calculated bulk chemical potentials and formation enthalpies of all investigated phases within PBEsol, along with their respective space groups [24].

System	Space group	μ^{bulk} (eV)	ΔH^f (eV)	System	Space group	μ^{bulk} (eV)	ΔH^f (eV)
K	$Im\bar{3}m$	–1.11	0	O		–4.57	0
KO_2	F4/mmm	–13.94	–3.68	P	Cmce	–5.78	0
KP	$P2_12_12_1$	–7.70	–0.81	P_2O_3	$P2_1/m$	–35.03	–9.74
KPO_3	$P2_1/c$	–34.06	–13.44	P_2O_5	Pnma	–51.65	–17.20
$KTiOPO_4$	Pnma	–62.68	–24.50	Ti	$P6_3/mmc$	–8.31	0
K_2O	$F4/m\bar{3}2/m$	–10.52	–3.72	TiO	$F4/m\bar{3}2/m$	–18.39	–5.51
K_2O_2	Cmce	–16.88	–5.51	TiO_2	Pbca (Brookite)	–27.99	–10.53
K_2P_3	Fmmm	–21.59	–2.02	TiO_2	$P4_2/mmm$ (Rutile)	–27.95	–10.50
K_2P_3	Fddd	–21.59	–2.02	TiO_2	$I4_1/amd$ (Anatase)	–28.01	–10.55
K_2TiO_3	Cmcm	–40.84	–16.59	TiP	$P6_3/mmc$	–16.61	–2.51
$K_2Ti_2O_5$	C2/m	–69.16	–27.45	TiP_2O_7	$P2_1/c$	–81.69	–29.79
$K_2Ti_6O_{13}$	C2/m	–182.22	–70.68	Ti_2O	$P\bar{3}m1$	–27.54	–6.35
K_3PO_4	Pnma	–47.73	–20.32	Ti_2O_3	$P2_1/m$	–47.16	–16.82
$K_3Ti_8O_{17}$	$P\bar{1}$	–240.63	–93.07	Ti_3O	$P\bar{3}1c$	–36.05	–6.55
$K_4P_2O_7$	$P6_3/mmc$	–81.91	–33.88	Ti_3O	P312	–35.62	–6.12
K_4P_3	Cmcm	–24.32	–2.53	Ti_3O_5	C2/m	–75.24	–27.44
K_4TiO_4	$P\bar{1}$	–52.33	–21.28	Ti_6O	$P\bar{3}$	–61.13	–6.71
$K_6Ti_2O_7$	$P2_1/c$	–93.19	–37.89	Ti_7P_4	C2/m	–94.65	–13.35

Therefore, a symmetric material slab consisting of 7 bulk, 8 surface, and 2 termination layers is chosen to model the surface, see Fig. 2.

The various combinations of $i, j, k,$ and l in the KTP surface stoichiometry $K_iTi_jP_kO_l$ for the Z^+-, Z^--, and Y-cut surfaces gives rise to a large number of possible surface terminations. More than 500 of those were explored in the present study. In particular we focus on O-rich surface structures that turned out to be particularly favorable in the calculations.

Ab initio thermodynamics, see e.g., Refs. [15,25,26] is used to determine the most favorable surface structures. Here it is aimed at determining the configurations that minimize the surface free energy

$$\gamma = \frac{\Omega(T, \{\mu_i\})}{A}, \tag{1}$$

with respect to the chemical potentials $\{\mu_i\}$ of atomic species i. The surface area and the grand canonical potential, respectively, are denoted by A and $\Omega(T, \{\mu_i\})$. The latter is approximated as

$$\Omega(\{\mu_i\}) \approx E_{\text{DFT}}(\{N_i\}) - \sum_i \mu_i N_i, \tag{2}$$

where $E_{\text{DFT}}(\{N_i\})$ corresponds to the DFT ground-state energy of a system consisting of N_i atoms of element i. Several side conditions must be fulfilled by the set $\{\mu_i\}$ in order to ensure the KTP thermodynamic stability. The chemical potentials cannot be chosen independently, but are related to the KTP heat of formation (see Table I),

$$\Delta\mu_K + \Delta\mu_{Ti} + \Delta\mu_P + 5\Delta\mu_O = \Delta H^f_{KTP}, \tag{3}$$

where

$$\Delta H^f_{KTP} = \mu^{\text{bulk}}_{KTP} - \mu^{\text{bulk}}_K - \mu^{\text{bulk}}_{Ti} - \mu^{\text{bulk}}_P - 5\mu^{\text{bulk}}_O. \tag{4}$$

Here $\Delta\mu_i = \mu_i - \mu_i^{\text{bulk}}$ denotes the chemical potential variation with respect to the bulk phase of element i. In case of K, Ti, and P the bulk phases are given by bcc potassium [27], hcp titanium [28], and black phosphorus [29]. Molecular oxygen O_2 is assumed to be the O reservoir. The respective μ_i^{bulk} values are determined by the ground-state energy per formula unit of the respective phase. The values calculated in the present study within DFT-PBEsol are compiled in Table I. Furthermore, in order to prevent KTP segregation into the bulk phases of its constituents, the following condition must be met

$$\Delta H^f_{KTP} \leqslant \Delta\mu_i \leqslant 0; \quad i \in \{K,Ti,P\}$$
$$\text{and} \quad \Delta H^f_{KTP} \leqslant 5\Delta\mu_O \leqslant 0. \tag{5}$$

This effectively limits the range of the individual chemical potentials. In order to reduce the degrees of freedom for the surface chemical potentials, $\Delta\mu_O$ is, in the following, considered fixed via the pressure and temperature dependent expression for the chemical potential of an ideal diatomic gas [30]:

$$\Delta\mu_O(p,T) = \frac{k_BT}{2}\left[\ln\left(\frac{p\lambda^3}{k_BT}\right) - \ln(Z_{\text{rot}}) - \ln(Z_{\text{vib}})\right] \tag{6}$$

with

$$\lambda = \sqrt{\frac{2\pi\hbar^2}{mk_BT}} \tag{7}$$

as the de Broglie wavelength of O_2 and Z_{rot}, Z_{vib} as the rotational and vibrational partition functions, respectively. Assuming $T = 300$ K and ultrahigh vacuum (UHV) conditions, $\Delta\mu_O$ amounts to -0.69 eV. Ending up with three degrees of freedom ($\Delta\mu_K$, $\Delta\mu_{Ti}$, and $\Delta\mu_P$), the surface stability may be explored using ternary phase diagrams, see Fig. 3. Each point in this graph thereby corresponds to three values for $\{\Delta\mu_K, \Delta\mu_P, \Delta\mu_O\}$ that obey Eq. (5). Further conditions on the chemical potentials are derived from the assertion that no segregation into biatomic A_iB_j or triatomic $A_iB_jC_k$ phases should occur, i.e.,

$$i\cdot\Delta\mu_A + j\cdot\Delta\mu_B + k\cdot\Delta\mu_C \leqslant \Delta H^f_{A_iB_jC_k}, \tag{8}$$

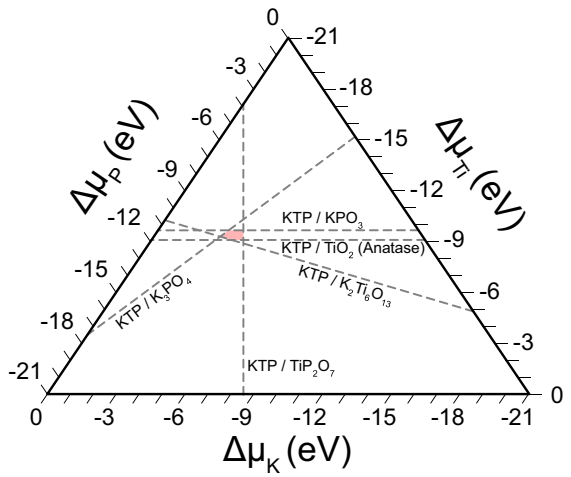

FIG. 3. Binodal curves within the KTP phase diagram, directly enclosing the stability region for bulk KTP formation, indicated in red (see text).

for A,B,C ∈ {K,Ti,P,O}. In case of four elements, Eq. (8) implies a series of conditions for a vast number of stable bi- and triatomic compounds. In our study, we focused on 31 compounds, whose formation enthalpies (after structural relaxation) are summarized in Table I. Fulfilling all conditions simultaneously implies a restriction to the full accessible phase space $\{\Delta\mu_i\}$, given by Eq. (5). In Fig. 3 the ternary phase space is visualized along with the bulk KTP stability range. The latter is given by the intersection of all binodal curves partitioning the phase space according to Eq. (8).

III. RESULTS

The calculated phase diagrams of Z^+ and Z^- surfaces are shown in Fig. 4, bottom. Both cuts show a large variety of stable surface terminations in dependence on the chemical potentials of the surface constituents, i.e., the surface preparation conditions. Interestingly, bulk terminated $K_2Ti_2P_2O_4$ and O_6 surfaces are not among the stable surfaces, stable terminations closest to bulk cut stoichiometries are found to be $O_3(y_O)$ and $K_2P_2O_3(y)$. In general, the energy differences between the energetically most favored terminations at each point of the phase diagram are found to be very small, typically of the order of a few 100 meV. This holds also for the energy differences between most x- and y-type terminations of equal stoichiometry. For this reason, temperature effects as well as kinetic effects related to the surface preparation conditions can be expected to have a noticeable influence on the surfaces experimentally observed. As a general trend, x_O as well as y_O terminations are very unfavorable for both the Z^+ and the Z^- cut, with the exception of a small region of stable O_3 (y_O) reconstructions on both cuts. Moreover, with the exception of $K_2(y)$, all terminations within the stability region of both Z

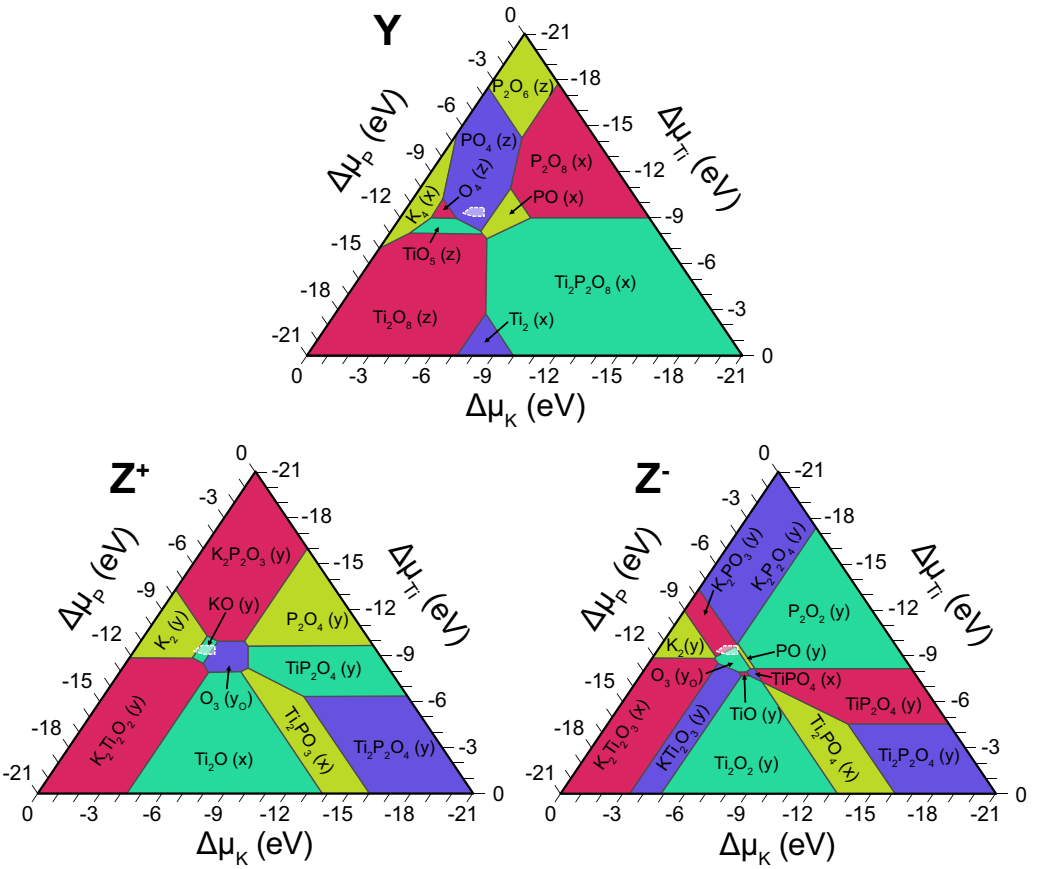

FIG. 4. Phase diagrams of KTP Y-cut (up), Z^+ (left), and Z^- (right) surfaces. Bulk stability region is sketched in white. UHV conditions have been assumed in order to determine the chemical potential of oxygen.

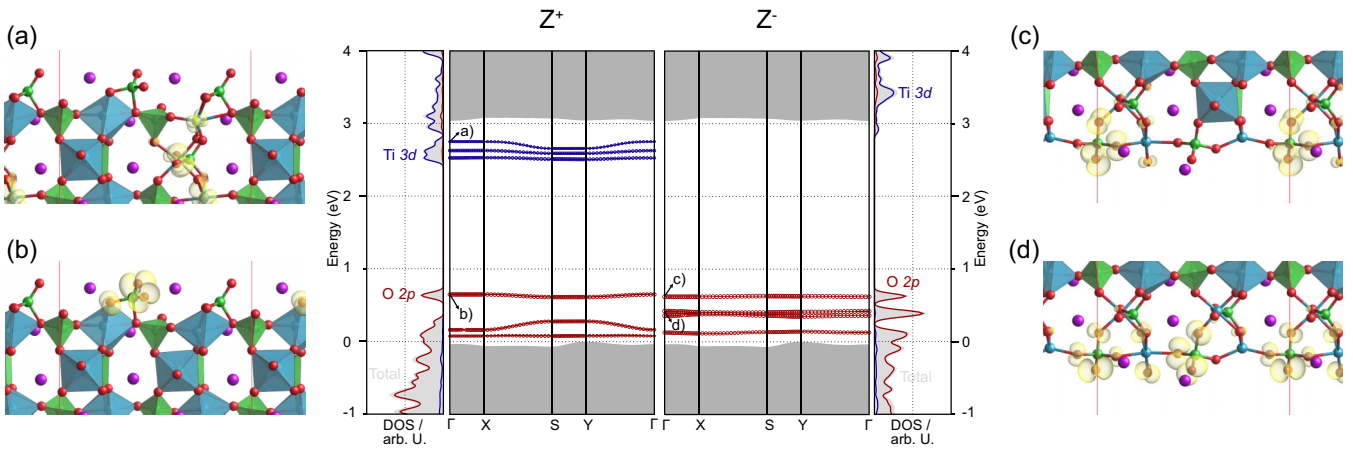

FIG. 5. Left: Localized surface states of $K_2P_2O_3$(y) termination on the Z^+ surface. Right: Localized surface states of $O_3(y_O)$ on the Z^- surface. Blue Ti 3*d* states are empty, while red O 2*p* states are occupied. Shaded area indicates KTP bulk band structure. Size of the circles correspond to the degree of localization within the first surface layers. Charge densities of Ti 3*d* and O 2*p* derived surface states are depicted in (a)–(d).

cuts are O rich. No Ti terminated surface structures are found to occur within the KTP stability region.

Two main structural motifs can be identified for stable Z^+ and Z^- terminations. On the one hand, for stable terminations involving phosphorous, P and O atoms tend to arrange in a way that preserves the fourfold coordination of P. This is exemplary shown for $K_2P_2O_3$(y) on Z^+ in Fig. 5(a) and $O_3(y_O)$ on Z^- in Fig. 5(c). On the other hand, it is observed that an increase of unsaturated O bonds leads to a strong outward relaxation of K atoms from the inner layer. This can be explained by the Coulomb attraction that affects the alkali ions.

Apart from the similarities between Z^+ and Z^- surfaces discussed above, there are also strong differences, especially regarding the amount of stable terminations. On Z^- a number of terminations [PO(y), TiO(y), and $TiPO_4$(x)] are found to be stable only for a very small regions within the phase space. Additionally, terminations on Z^- are found, on average, to

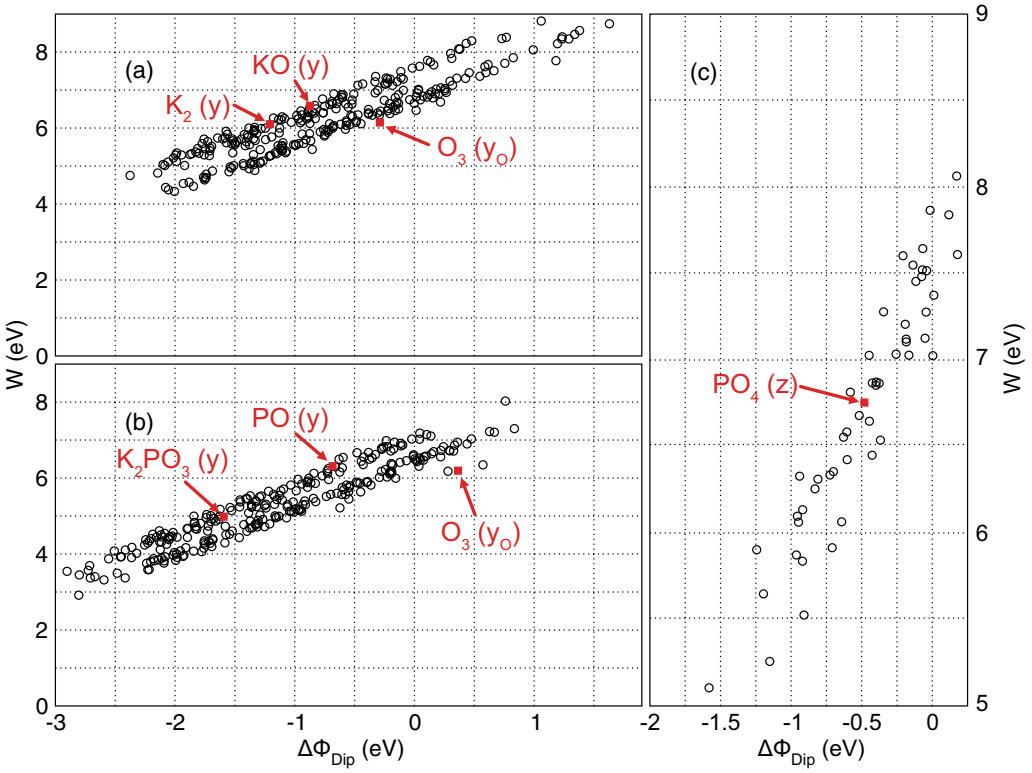

FIG. 6. Work functions *W* and relative change of the surface dipole $\Delta\Phi_{Dip}$ (see text) of all investigated terminations for (a) Z^+, (b) Z^-, and (c) Y-cut surfaces. Stable surfaces are highlighted in red.

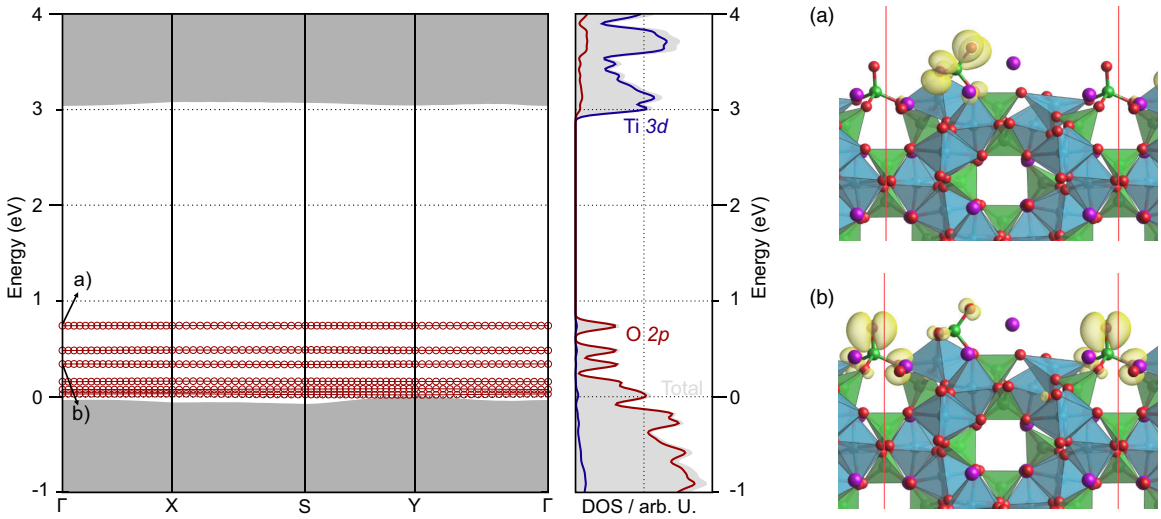

FIG. 7. Surface band structure of PO_4(z) termination on KTP y-cut. Shaded area indicates KTP bulk band structure. Size of the circles correspond to the degree of localization within the first surface layers. Charge densities of the occupied O $2p$ surface states are depicted in (a) and (b), respectively.

feature a higher O coverage compared to Z^+. Thus, Z^+ and Z^- differ not only with respect to the orientation of the bulk polarization direction, but also with respect to the surface stoichiometry.

The calculated stoichiometries appear to be at variance with experimental reports indicating essentially a bulk-like composition of KTP surfaces [18,19]. However, it is not clear wether the mechanical polishing applied to the substrates indeed leads to surfaces in thermodynamic equilibrium.

The stoichiometry changes, rebonding processes and structural modifications accompanying the KTP surface formations modify the materials electronic properties. In particular O_{2p} related states appear in the region of the KTP bulk band gap. Occupied oxygen states are pushed above the KTP valence-band maximum (VBM) in the cases of the Z^+ $K_2P_2O_3$(y) surface [see Fig. 5(b)] and the Z^- $O_3(y_O)$ surface [see Fig. 5(c)]. In the former case, unoccupied Ti_{3d} states, originating from Ti atoms underneath the surface, appear below the KTP conduction-band minimum (CBM). This leads to a considerable shrinkage of the band gap to nearly half of its bulk value. In Figs. 6(a) and 6(b) work functions W as well as the changes of the surface dipoles $\Delta\Phi_{Dip}$ [with respect to the $K_2Ti_2P_2O_4$(y) surface] of all investigated terminations on Z^+ and Z^- are compiled. W is calculated here as difference between the KTP bulk VBM and the local potential within the vacuum region. The apparent shift between terminations of x and y type for both Z^+ and Z^- can be explained by the choice of a single reference for all termination types. As expected, W depends linearly on $\Delta\Phi_{Dip}$. Stable terminations within the KTP stability region on Z^- are found to show a stronger variation regarding the work function (4.98-6.31 eV) compared to Z^+ (6.1-6.6 eV).

The surface phase diagram of the KTP Y-cut is shown in the upper part of Fig. 4. Similar to the results for the Z-cuts discussed above, we find a tendency to form O-rich and Ti-poor surfaces. Solely the PO_4(z) termination is found to be most stable within the KTP stability region. Similar to the Z-cut, PO_4(z) is structurally characterized by the preservation of the fourfold coordination of P [shown in Fig. 7, right-hand side]. The surface band structure of the stable surface features occupied surface states derived from O $2p$ orbitals that are energetically above the KTP bulk VBM, as shown in Fig. 7.

In Fig. 6(c) the work functions W and surface dipole changes $\Delta\Phi_{Dip}$ [relative to the $Ti_2P_2O_{12}$(z) surface] for all investigated Y-cut surfaces are shown. As expected, the work function changes linearly with the induced surface dipole in a range between 5.1 eV and 8.1 eV, with PO_4(z) falling in between at 6.75 eV.

IV. CONCLUSIONS

Surface phase diagrams of KTP Z- and Y-cut surfaces have been determined from density-functional theory calculations. The surfaces are characterized by various surface phases in dependence on the surface preparation conditions, i.e., the chemical potential values of the surface constituents. The energy differences between the competing phases are typically small, indicating a strong influence of thermal and kinetic effects on the actual surface structure. Z^+ and Z^- surfaces show differences with respect to the equilibrium surface structures. Nevertheless, there are common trends that hold for all surfaces investigated. (i) The surfaces tend to be O-rich and Ti-poor. (ii) Fourfold coordinated P atoms are a structural motif typical for all surfaces. (iii) On average, stable Z^- surfaces are characterized by a higher O content than Z^+ surfaces. (iv) Surface states, predominantly derived from occupied O $2p$ states and empty Ti $3d$ states, occur in the region of the KTP bulk band gap and reduce the minimum transition energy with respect to the bulk material.

ACKNOWLEDGMENTS

Financial support by DFG (SCHM1361/25, SCHM1361/26, TRR 142 Project No. 231447078)

is gratefully acknowledged. The authors thank the Paderborn Center for Parallel Computing (PC^2) and the Höchstleistungs-Rechenzentrum Stuttgart (HLRS) for Grants of high-performance computer time.

[1] L. K. Cheng and J. D. Bierlein, Ferroelectrics **142**, 209 (1993).
[2] J. D. Bierlein and H. Vanherzeele, J. Opt. Soc. Am. B **6**, 622 (1989).
[3] M. Roth, N. Angert, and M. Tseitlin, in *Proceedings of the Second Israeli-Russian Binational Workshop* (Jerusalem, Tel-Aviv, 2003), pp. 223–235.
[4] P. A. Thomas, A. M. Glazer, and B. E. Watts, Acta Crystallogr. Sect. B **46**, 333 (1990).
[5] D. Xue and S. Zhang, Appl. Phys. Lett. **70**, 943 (1997).
[6] M. N. Satyanarayan, A. Deepthy, and H. L. Bhat, Crit. Rev. Solid State Mater. Sci. **24**, 103 (1999).
[7] C. Defan and Y. Zhengtang, J. Cryst. Growth **79**, 974 (1986).
[8] G. M. Loiacono, D. N. Loiacono, and R. A. Stolzenberger, J. Cryst. Growth **131**, 323 (1993).
[9] S. D. Setzler, K. T. Stevens, N. C. Fernelius, M. P. Scripsick, G. J. Edwards, and L. E. Halliburton, J. Phys.: Condens. Matter **15**, 3969 (2003).
[10] A. Bocchini, S. Neufeld, U. Gerstmann, and W. G. Schmidt, J. Phys.: Condens. Matter **31**, 385401 (2019).
[11] M. G. Roelofs, J. Appl. Phys. **65**, 4976 (1998).
[12] K. T. Stevens, N. C. Giles, and L. E. Halliburton, Appl. Phys. Lett. **68**, 897 (1998).
[13] G. Rosenman, A. Skliar, M. Oron, and M. Katz, J. Phys. D **30**, 277 (1997).
[14] G. Rosenman, A. Skliar, D. Eger, M. Oron, and M. Katz, Appl. Phys. Lett. **73**, 3650 (1998).
[15] S. Sanna and W. G. Schmidt, J. Phys.: Condens. Matter **29**, 413001 (2017).
[16] R. J. Bolt and W. J. P. van Enckevort, J. Cryst. Growth **119**, 329 (1992).
[17] I. V. Nikolaev, N. G. Korobeishchikov, and M. A. Roenko, J. Phys.: Conf. Ser. **1382**, 012162 (2019).
[18] V. V. Atuchin, V. G. Kesler, N. Y. Maklakova, L. D. Pokrovsky, and V. N. Semenenko, Surf. Interface Anal. **34**, 320 (2002).
[19] V. V. Atuchin, M. A. Litvinov, N. Y. Maklakova, L. D. Pokrovsky, V. N. Semenenko, and D. V. Sheglov, J. Struct. Chem. **45**, S84 (2004).
[20] G. Kresse and J. Furthmüller, Phys. Rev. B **54**, 11169 (1996).
[21] G. Kresse and D. Joubert, Phys. Rev. B **59**, 1758 (1999).
[22] J. P. Perdew, A. Ruzsinszky, G. I. Csonka, O. A. Vydrov, G. E. Scuseria, L. A. Constantin, X. Zhou, and K. Burke, Phys. Rev. Lett. **100**, 136406 (2008).
[23] S. Neufeld, A. Bocchini, U. Gerstmann, A. Schindlmayr, and W. G. Schmidt, J. Phys.: Mater. **2**, 045003 (2019).
[24] A. Jain, S. P. Ong, G. Hautier, W. Chen, W. D. Richards, S. Dacek, S. Cholia, D. Gunter, D. Skinner, G. Ceder, and K. A. Persson, APL Mater. **1**, 011002 (2013).
[25] S. J. Jenkins, Phys. Rev. B **70**, 245401 (2004).
[26] S. V. Levchenko and A. M. Rappe, Phys. Rev. Lett. **100**, 256101 (2008).
[27] L. G. Liu, J. Phys. Chem. Solids **47**, 1067 (1986).
[28] P. D. Hao, P. Chen, L. Deng, F. X. Li, J. H. Yi, D. Şopu, J. Eckert, J. M. Tao, Y. C. Liu, and R. Bao, J. Mater. Res. Technol. **9**, 3488 (2020).
[29] Y. Du, C. Ouyang, S. Shi, and M. Lei, J. Appl. Phys. **107**, 093718 (2010).
[30] I. A. R. Alvarado, M. Karmo, E. Runge, and W. G. Schmidt, ACS Omega **6**, 6297 (2021).